Journal of Engineering Science and Technology Review 16 (6) (2023) 185 - 194

Research Article

JOURNAL OF
Engineering Science and Technology Review

www.jestr.org

Failure Mechanism and Precursor Analysis of Foam Concrete Subgrade with Different Densities Based on Acoustic Emission Data

Chao Qi[1,2], Rong Liu[3,*], Jucai Chang[2], Lulu Gao[1,2] and Zhiqiang Yin[2,3]

[1]*Key Laboratory of Safety and High-Efficiency Coal Mining of Ministy of Education, Anhui University of Science and Technology, Huainan 232001, China*
[2]*School of Mining Engineering, Anhui University of Science and Technology, Huainan 232001, China*
[3]*Coal Mine Safety Mining Equipment Innovation Center of Anhui Province, Anhui University of Science and Technology, Huainan, 232001, China*

Received 29 August 2023; Accepted 15 December 2023

Abstract

The density of the formed concrete subgrade can be designed based on different working conditions in foam concrete backfilled soft subgrade. The stability of formed concrete with different densities is a critical factor that influences subgrade and pavement projects, and it is vital to traffic safety. Foam specimens with different densities were prepared to perform failure mechanisms and precursor analysis of foam concrete subgrade, and a vibration test was conducted using a vibration table. The critical failure precursors of formed concrete with different densities were analyzed by combining them with microscopic failure mechanisms. Results demonstrate that, as the density of the specimens increases, foam concrete subgrade presents progressive failure characteristics under vehicle loads. The peak of the acoustic emission b value increases from 2.1 to 2.9, and the large-scale fracture characteristics are weak at the early stage of specimen damage. By contrast, the small-scale fracture characteristics before the critical failure are enhanced gradually. With the increase in foam concrete density, the shear cracks at the initial damage stage play a dominant role because fiber cohesion mainly acts on early loading, resulting in the hysteresis effect of tensile failure. The primary frequency distribution characteristics of foam concrete with different densities are concluded through clustering recognition of acoustic emission parameters. The proposed novel method provides a significant evidence for the failure mechanism and precursor analysis of foam concrete subgrade with different densities through an organic combination of acoustic emission parameters and the microscopic failure mechanisms.

Keywords: Foam concrete subgrade, Failure characteristics, Fracture characteristics, Clustering

1. Introduction

Recently, highway construction frequently has encountered soft subgrade during the continuous extension of the highway traffic transportation network. Problems influencing driving comfort and safety frequently occur in a soft subgrade under service due to its excellent sedimentation rate and uneven sedimentation. Foam concrete has been widely applied in the backfilling of soft subgrade due to low weight, small density, controllable strength, and good curing independence [1, 2]. Given these advantages, according to traffic pavements conditions, the density and strength of foam concrete subgrade can be controlled through a reasonable design of additives with different proportions, bubble volumes, and cement contents. However, recent studies have demonstrated that the mechanical responses of foam concrete with different densities exhibit considerable differences due to the inconsistent internal aggregates, pores, and porosities [3-5]. Hence, studying the failure mechanisms and precursors of foam concrete subgrade with different densities has practical value.

Previous studies have reported that the preparation technology of foam concrete materials has become increasingly mature [6], and the application of foam concrete backfilled soft subgrade has become extensive. Profound studies on foam concrete's failure mechanisms and failure precursors have become a core demand to control foam concrete backfilled subgrade. Concerning the failure mechanisms and failure characteristics of foam concrete, many scholars have investigated the uniaxial compressive strength [7], triaxial compressive strength [8], tensile strength [9], shear strength [10], and bending strength of foam concrete materials [11]. However, foam concrete with different densities has different damage modes and evolutionary characteristics [12, 13]. Therefore, foam concrete subgrade with different densities needs to be investigated by considering microscopic failure mechanisms. Precursor analysis of foam concrete usually employs an acceleration sensor [14], a displacement sensor [15], the ultrasonic pulse transmission method [16], and ultrasonic chromatography [17]. However, acceleration and displacement sensors involve single measurement variables when monitoring of foam concrete subgrade, and their usage cannot be promoted. The ultrasonic pulse transmission method and ultrasonic chromatography have complicated working processes and low efficiency, so it is difficult to provide a real-time reflection of the internal damage evolution of foam concrete is difficult.

With the development of non-destructive testing technology, acoustic emission (AE) has been applied to the damage monitoring of foam concrete [18]. At present, AE is mainly utilized to monitor amplitudes and ringing changes in foam concrete in the loading process and reflect the failure mode and crack propagation of foam concrete. The failure

*E-mail address: qianxunsen@163.com
ISSN: 1791-2377
doi:10.25103/jestr.166.23

precursors of foam concrete with different densities need to be further analyzed based on AE parameters, and the characteristic ranges of their critical failure parameters must be determined. Furthermore, a precursor recognition novel method for critical failure needs to be developed, and the deformation and failure of foam concrete subgrade must be controlled.

On this basis, foam concrete subgrade specimens with different densities are prepared, and damage mechanisms are analyzed. The crack evolutionary laws are analyzed by combining microscopic failure mechanisms and the novel method to recognize the fracture precursors of foam concrete subgrade. The results lay an experimental foundation for new foam concrete backfilled soft subgrades.

2. State of the art

Many scholars have studied the failure mechanisms and precursors of foam concrete with different densities. Focusing on the failure mechanism of foam concrete with different densities, Hao et al. [19] designed activated foam concrete with a density ranging within 200-1200 kg/m^3 and found that with the increase in specimen density, the compressive strength increased from 0.5 MPa to 44.98 MPa, and the bending strength increased from 0.22 MPa to 13.86 MPa. Falliano et al. [20] prepared foam concrete specimens with different densities by using different foaming agents. They found that foaming agents influenced the density of foam concrete, resulting in differences in foam concrete strength. Song et al. [21] tested the elasticity modulus of foam concrete with a density of 400-800 kg/m^3 by using resonance frequency and found that the failure process of foam concrete included phase-linear elastic, transition, plateau, and densification stages. They also constructed the constitutive relation between elasticity modulus and foam concrete strength. Zhao et al. [22] discussed the effects of fiber on the mechanical properties and mechanisms of foam concrete with a dry density of 300-800 kg/m^3. Their foam concrete compression curve model mainly comprised elastic, brittle, and yield stages. They reported that the compressive strength, elasticity modulus, and tensile strength of foam concrete increased as the density increased. Moreover, foam concrete's comprehensive strength, elasticity modulus, and bending strength increased initially and then decreased as the fiber content increased. Gökçe et al. [23] conducted a compressive test on foam concrete with different densities and found that low-density foam concrete had some strain hardening capacity due to the abundant internal pores. However, high-density specimens fail in strain softening, and the fiber distribution in the substrate became increasingly uniform because of the reduction in foam content. To sum up, previous studies focused on single mechanical responses of foam concrete. The damage mechanism of foam concrete with different densities varies under the action of external loads, and foam concrete's internal microscopic failure mechanisms remain unclear. Hence, the failure mechanisms of foam concrete with different densities need to be examined by combining the microscopic damage mechanisms.

For a precursor analysis of foam concrete with different densities, De Sutter et al. [24] studied fracture behaviors of a carbon fiber-reinforced polymer mixed foam concrete beam through AE. They found that in the fixed failure mode, the AE parameters of the specimens remained stable, and the foam concrete beam presented a more extended low-frequency AE waveform compared with that of pure cement substrate cracking. Rasheed et al. [25] discussed the failure process of fiber-reinforced cellular concrete through AE. According to the test results, AE and shear fracture energy increased with the increase in fiber content, and structural synthetic fiber increased the ultimate shear strength of cellular concrete considerably. The researchers also evaluated the crack patterns of foam concrete in accordance with the AE parameters. Based on the AE monitoring technology, Lin et al. [26] conducted a quasi-static cyclic loading compression test on foaming polymers, such as foam concrete, and classified the failure modes by using the data of AE parameters. An energy-based constitutive damage factor analysis was also conducted using AE parameter energy. Li et al. [27] investigated the compressive failure characteristics of foam concrete with densities ranging within 500-750 kg/m^3 and summarized the variation characteristics of their AE parameters. They found that the activity of AE signals increased before the peak, and the ringing count increased suddenly and became increasingly concentrated at the failure of foam concrete. However, existing studies that performed precursor analyses of foam concrete mainly evaluated macroscopic failure mechanisms by using data of AE parameters. Only a few studies have been conducted on precursor failure information (e.g., dominant frequency distribution) through an organic combination of AE parameters and foam concrete damages. Therefore, how to accurately predict the precursor information of foam concrete subgrade at different damage stages by combining microscopic failure mechanisms is an urgent problem that has to be solved.

In this study, foam concrete specimens with different densities (400, 500, 600, and 700 kg/m^3) are prepared based on foam concrete backfilled soft subgrade to address the shortages of existing studies. Vibration failure tests are conducted on foam concrete with different densities. The AE system is applied for parallel monitoring of vibration damages of the prepared foam concrete specimens, and the failure mode of the foam concrete subgrade is determined. The critical failure precursors of foam concrete subgrade are analyzed by combining them with microscopic failure mechanisms. The results provide an experimental reference for the analysis of the failure mechanisms and precursors of foam concrete subgrades with different densities.

The remainder of this study is organized as follows. Section 3 introduces the experimental apparatus and test method. Section 4 analyzes the vibration AE signals of foam concrete subgrades with different densities, discusses the staged damage characteristics and damage modes of specimens, and examines the failure precursors. Section 5 summarizes the research results and relevant conclusions.

3. Methodology

3.1 Preparation of specimens

Foam concrete specimens with density levels of 400, 500, 600, and 700 kg/m^3 are prepared using the physical foaming technique. The preparation process is as follows: cement, water, a foaming agent, and fiber are mixed at certain ratios. The foaming agent is added, stirred, and poured uniformly. The mixing ratios of the foam concrete specimens with different densities are listed in Table 1. Some finished specimens are shown in Fig. 1.

Table 1. Mix ratios of foam concrete with different densities

Density /kg/m^3	Cement /kg/m^3	Water /kg/m^3	Foaming Agent /kg/m^3	Fiber-Content /%
400	244	130	0.59	0.5
500	297	173	0.55	0.5
600	355	216	0.53	0.5
700	430	240	0.49	0.5

Fig. 1. Schematic of the finished specimens

3.2 Experimental apparatus

In this study, a sinusoidal vibration test is designed to simulate the vehicle load vibration environment of the foam concrete subgrade [28]. The self-made, clamp-fixed specimens are subjected to vibration excitation loads applied by a vibration table through the sinusoidal excitation output of the controller. The data acquisition device performs a real-time collection of vibration table data. In this way, closed-loop control is realized. Data, such as AE amplitude and the energy and count of foam concrete, are collected in real time by the AE probe, which is pasted onto the specimen surface. The damage mechanism of the foam concrete specimens throughout the vibration test is monitored. The minimum threshold of noises is filtered in advance under idle running conditions to decrease the interference of noises. In this experiment, the threshold is 26 dB. The pre-amplification gain and sampling frequency are 40 dB and 10 MHz, respectively. Before the experiment, Vaseline is used to couple the probes and specimens. The whole test process is shown in Fig. 2.

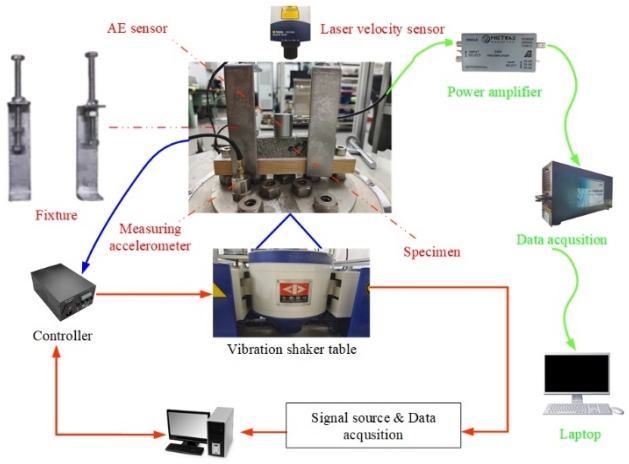

Fig. 2. Test process

3.3 Loading frequency

The vibration excitation caused by low-frequency modal resonance may lead to a fold increase in the dynamic responses of the exciter. The first-order inherent frequency is used to test the foam concrete subgrade structure and reduce the vibration responses of the foam concrete subgrade to the maximum extent. Before the test, sweep frequency is performed to determine the first-order intrinsic frequency of foam concrete subgrade.

Sweep frequency is performed using a linear upward sweep frequency mode. Concrete specimens are fixed onto the vibration table through a clamp, and the laser dot of the speed sensor is applied to the concrete surface. The focal length of the sensor lens is adjusted to make the energy threshold of the laser dot exceed 1/3. Given some excitation energy, the foam concrete specimens' vibration speed response signals are acquired through the laser speed sensor and analyzed by speed mutation discrimination to obtain the resonance frequency of the specimens. The sweep frequency result of the specimens with a density of 500 kg/m^3 is shown in Fig. 3.

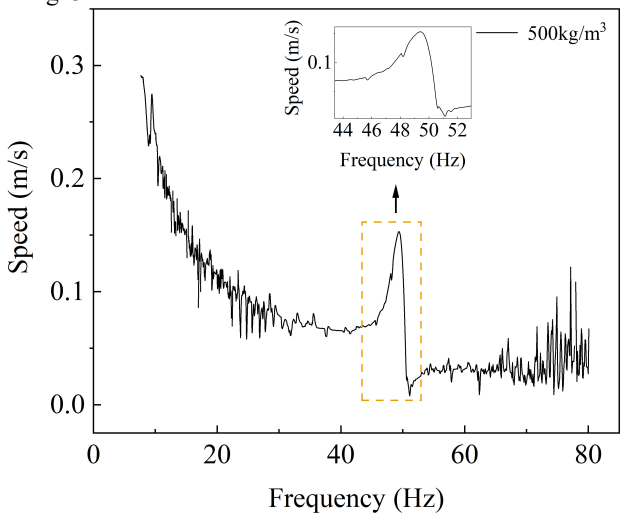

Fig. 3. Experimental results of sweep frequency

Fig. 3 indicates that specimen speed decreases gradually in the frequency interval of 5-40 Hz. When the excitation frequency of the sweep frequency approaches the resonance frequency, the vibration amplitude of the concrete specimens increases, and the vibration period decreases, resulting in a sharp increase in speed. When the inherent frequency is reached, the speed of the concrete specimens reaches the peak point and then begins to decrease suddenly until the sweep frequency test is finished. In accordance with the speed peak point, the inherent frequency of the concrete specimens is determined to be 49 Hz. The first-order sinusoidal sweep frequencies of the foam concrete specimens with densities of 400, 600, and 700 kg/m^3 under the test conditions are 32, 55, and 71 Hz, respectively.

4. Result analysis and discussion

4.1 Staged damage evolutionary characteristics of the foam concrete specimens with different densities

AE ringing count and amplitude reflect the times and amplitude that AE signals exceed the threshold value in unit time [29, 30]. They are closely related to the internal microcrack damage propagation of specimens. The ringing count and amplitude of the AE signals are analyzed to investigate the damage evolution of foam concrete with different densities during vibration under vehicle loads. The differences in AE amplitudes and counts under four density values are compared, and the internal damage variation laws of the foam concrete specimens with different densities are analyzed, as shown in Fig. 4.

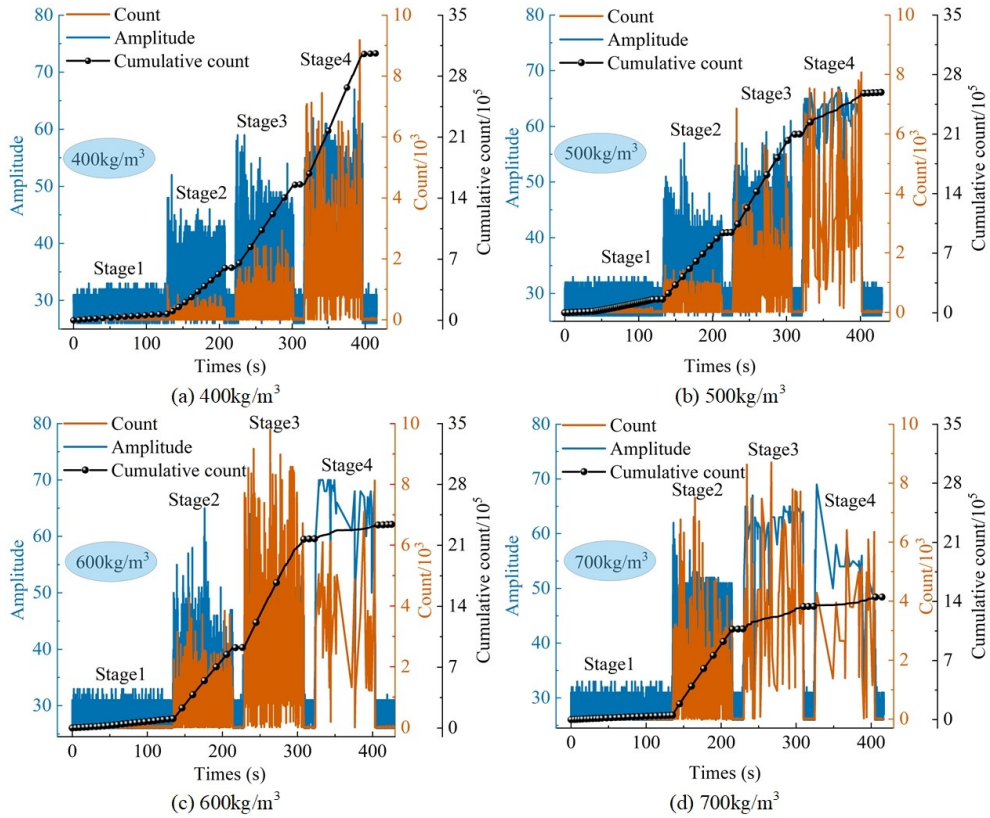

Fig. 4. Variation characteristics of acoustic emission amplitude, count, and cumulative count of foam concrete with different densities over time

As shown in Fig. 4, the damage of the foam concrete specimens with different densities can be stably divided into four stages: initial, stable, acceleration, and unstable damage stages. In the sinusoidal loading process, the ringing count of the specimens increases suddenly, and the cumulative ringing count presents stepped growth accompanied by prominent staged damage characteristics. The AE ringing count of the foam concrete specimens with different densities is constant at the initial damage stage when the amplitude fluctuates around the preset threshold. At this stage, the cumulative count is kept stable, and the specimen substrates develop frictional cracks in the vibration process. Only dense, low-energy events occur. At the stable damage stage, the ringing count and amplitude increase, accompanied by the notable growth of cumulative ringing count. These phenomena can be interpreted well by combining them with the scanning electron microscopy (SEM) results. The specimen with a 500 kg/m^3 density is adopted as an example. As shown in Fig. 5, the internal foam cellular connection structures begin to collapse, and the acoustic signals are enhanced as a response to the excitation of the vibration table because of the sliding of the substrate. As the deterioration degree of the specimens further increases, the amplitude and ringing count increase sharply. High-energy signals, such as fiber pull-out, are produced in a cluster when internal defects develop strongly in the specimens, indicating that the behavior changes from the stable damage stage to the acceleration damage stage. The load transfer paths of the specimens at the unstable damage stage depend on the transformation from the storage energy of cellular structures that have not been broken completely into energy released from macro-crack development. The cumulative energy of the continuous vibration of the specimens is released through the crack tips. At the same time, macro-cracks continue to propagate along the fracture surface of the cellular structures until the end of the specimen cracking test.

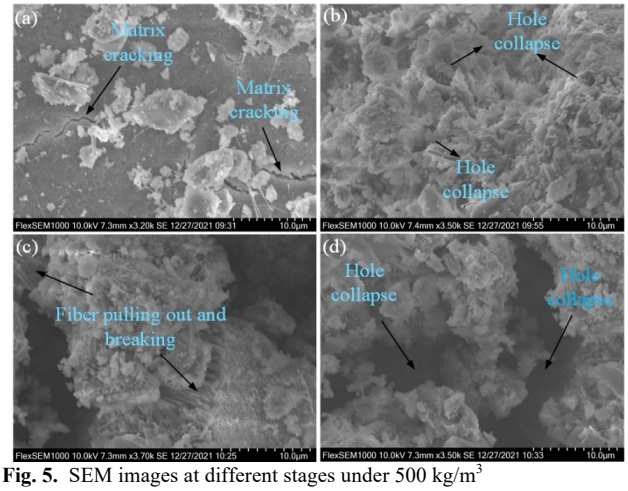

Fig. 5. SEM images at different stages under 500 kg/m^3

The ringing and cumulative ringing counts of the foam concrete specimens with different densities exhibit considerable differences, which are mainly manifested at the acceleration and unstable damage stages. At the two stages, the AE signals representation ability of the high-density specimens is poorer than that of the low-density specimens. According to the analysis, the AE signals are characterized by sudden energy changes. Obtaining AE signals with prominent performance requires the breakage of internal fibers and large-scale collapse of the cellular connection structure in foam concrete, thus generating high-energy signals. Low-density specimens have low cellular connectivity strength and can continuously produce high-energy signals. High-density specimens have tight cavity connections, and the vibration cumulative elastic energy has to reach some extent to break the internal fiber cohesion and

damage the cavity. As a result, acceleration and unstable damage stages will have few high-energy signals if the specimens have high densities. In this study, the foam concrete subgrade presents prominent progressive failure characteristics under vehicle vibration loads with the increase in the density of the foam concrete specimens.

4.2 Scale fracture characteristics of foam concrete with different densities

The AE b value is a statistical relation equation between earthquake magnitude and frequency proposed by Gutenberg and Richter [31], and it can be used as a criterion for judging crack initiation and development [32]. The AE b value is closely related to the specimen's crack. Many weak AE events occur when the b value is high. When the b value is constant, crack development is stable, and large and small cracks present a uniform development. When the b value is small, large cracks or sudden increments in crack propagation speed occur in rocks. The b value is calculated by the maximum likelihood estimation method as follows:

$$b = \frac{20 \lg e}{\bar{A} - A_{\min}} \tag{1}$$

where $\bar{A}$ is the average amplitude and $A_{\min}$ is the minimum earthquake magnitude.

A statistical analysis of the b value of the foam concrete specimens with different densities is performed with a sliding time step of 20 s. The statistical results of the b value are compared with those of AE energy to obtain the scale fracture characteristics of the foam concrete specimens under vehicle loads (Fig. 6).

Fig. 6 shows that the b value in the vibration tests on the foam concrete specimens with different densities exhibits good consistency with the energy release characteristics in the loading process. The b value presents a W-shaped variation in the whole process and generally shows characteristics of "fluctuation-decrease-increase-decrease." The b value of foam concrete fluctuates up and down in 0-130 s; the small-scale microcrack failure plays the dominant role and is accompanied with the frequent occurrence of low-energy events and crack initiation-propagation in the samples. The high-energy signals increase gradually within 130-220 s, and the b value decreases sharply and then increases. The vibration facilitates the development of internal cracks in the substrate, and the connection of the microcracks plays a dominant role. The AE b value decreases initially and then increases from 220 s to 320 s. The microcracks propagate continuously, inducing high-density occurrences of many high-energy events. The crack tips collide mutually. The specimens generally deteriorate due to the separated solid and weak phases and fiber bundle breakage. The b value decreases gradually from 320 s to 420 s, indicating that the foam concrete specimens develop large-scale macro-cracks, and fissures propagate continuously along the stress concentration tips until specimen breakage.

The peak point of the b value at the initial damage stage increases gradually from 2.1 to 2.9 when the density of the specimens increases from 400 kg/m^3 to 700 kg/m^3. This result demonstrates that with the increase in density, the shock strength of the specimens also presents a positively correlated progressive increase, and the tip failure effect of crack propagation weakens because of micro-crack initiation at the early internal damage stage of the specimens. As the density of the foam concrete specimens increases, the AE signal energy increases gradually at the stable and acceleration damage stages. The specimen with high density has high energy, and its b value at the stable damage stage decreases considerably. The shock strength of foam concrete is positively related to density. Meanwhile, the crack propagation scale is grand, and the macro-crack damage development characteristics are highly evident from the initial damage stage to the stable damage stage under the high density of the foam concrete specimens. The b value of the specimen with a density of 700 kg/m^3 increases from the stable damage stage to the acceleration and unstable damage stages. According to the analysis, the high-density specimens have the highest strength under vibration loads among all the specimens and it is dominated by strengthened AE signals caused by the tensile failure of fibers from the stable damage stage to the unstable damage stage. Therefore, the small-scale progressive failure characteristics before the critical failures of vehicle loads are gradually enhanced with the density of the foam concrete specimens.

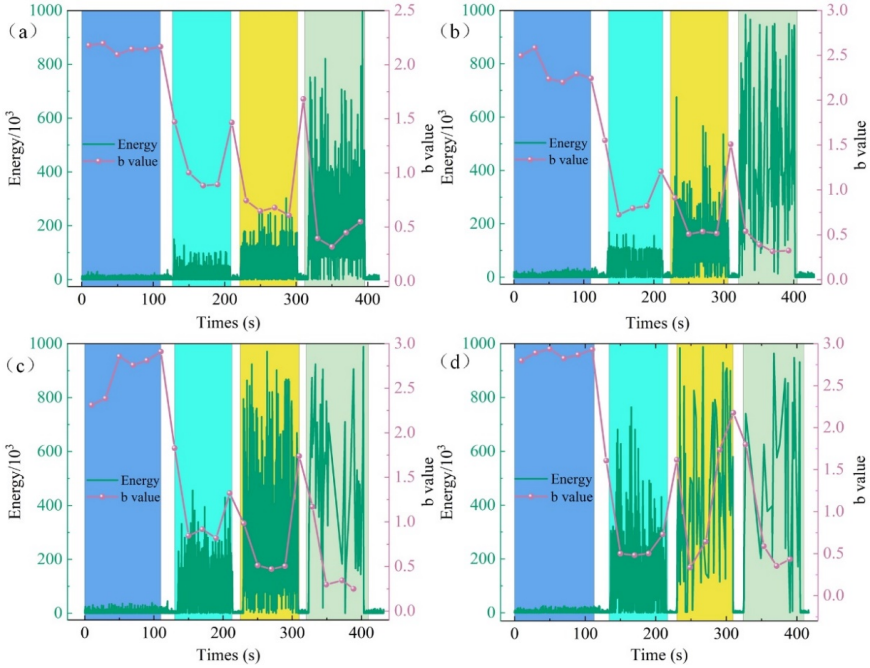

Fig. 6. Evolution characteristics of the acoustic emission energy and b value of foam concrete specimens with different densities

4.3 Crack damage mode of foam concrete with different densities

RA (Rise-Time/Amplitude Ratio) and AF (Average Frequency) are used as stability evaluation methods of shear tensile crack discrimination in the failure process of samples [33, 34]. Shear cracks have low elastic resilience. Shear cracks also have low AF and high RA due to the long rising time and duration period and small amplitude. Tensile cracks show the opposite. A scatter diagram of shear and tensile cracks is plotted (Fig. 7), in which a diagonal is drawn using the AF/RA ratio as the threshold. The cracks above the diagonal are tensile, and those below the diagonal are shear.

Fig. 7 shows that for the specimens with 400 kg/m^3, the tensile cracks are mainly distributed within a density of 0-40 kHz at the initial damage stage, and the shear cracks are mainly distributed within 10 kHz. The average frequency of the tensile cracks decreases gradually and approaches the origin with the continuous action of vibration excitation. The tensile crack frequency increases gradually at the stable, acceleration, and unstable damage stages because energy is released due to the mutual collision of crack tips in the damage process, thus endowing the high-frequency tensile cracks a dominant role. The RA-AF evolution diagram of the foam concrete with 500 kg/m^3 shows that the scatter point distribution is similar to that of the specimen with a density of 400 kg/m^3. RA approaches the origin gradually at the acceleration and unstable damage stages, and it is mainly distributed within 5-60 ms•V^{-1}. The number of high-amplitude events increases gradually, and the duration period declines due to the increase in the density of the specimens. According to the statistics on the scatter event numbers of the specimens with different densities (400 and 500 kg/m^3), tensile cracks dominate the initial and unstable damage stages. By contrast, shear cracks have the dominant role at the stable and acceleration damage stages. This finding can be interpreted as follows: most of the AE signals are caused by substrate friction in the vibration process of the initial damage stage. The cells in the internal matrixes of foam concrete begin to collapse, and fiber and fiber bundles break after entering the stable and acceleration damage stages. As a result, shear cracks account for the largest proportion among all the cracks. After entering the unstable damage stage, the cells that lose their fiber bundle cohesion break at a large scale, and the specimens show the failure mode of inconsistent horizontal collision and squeezing. The acceleration excitation perpendicular to the axial direction of the specimens acts on the specimen, resulting in the dominant role of tensile failures.

Compared with the specimens with different densities of 400 and 500 kg/m^3, the specimen with a density of 600 kg/m^3 has a relatively high tensile average frequency at the initial and stable damage stages. The tensile frequency is mainly distributed within 0-80 kHz. The RA value decreases gradually at the unstable damage stage and is mainly located within 0-40 ms•V^{-1}. The RA-AF evolutionary characteristic diagram of the scatter points of the specimen with a density of 700 kg/m^3 shows that the total number of microcrack events in the high-density specimens is lower smaller than that in the low-density specimens.

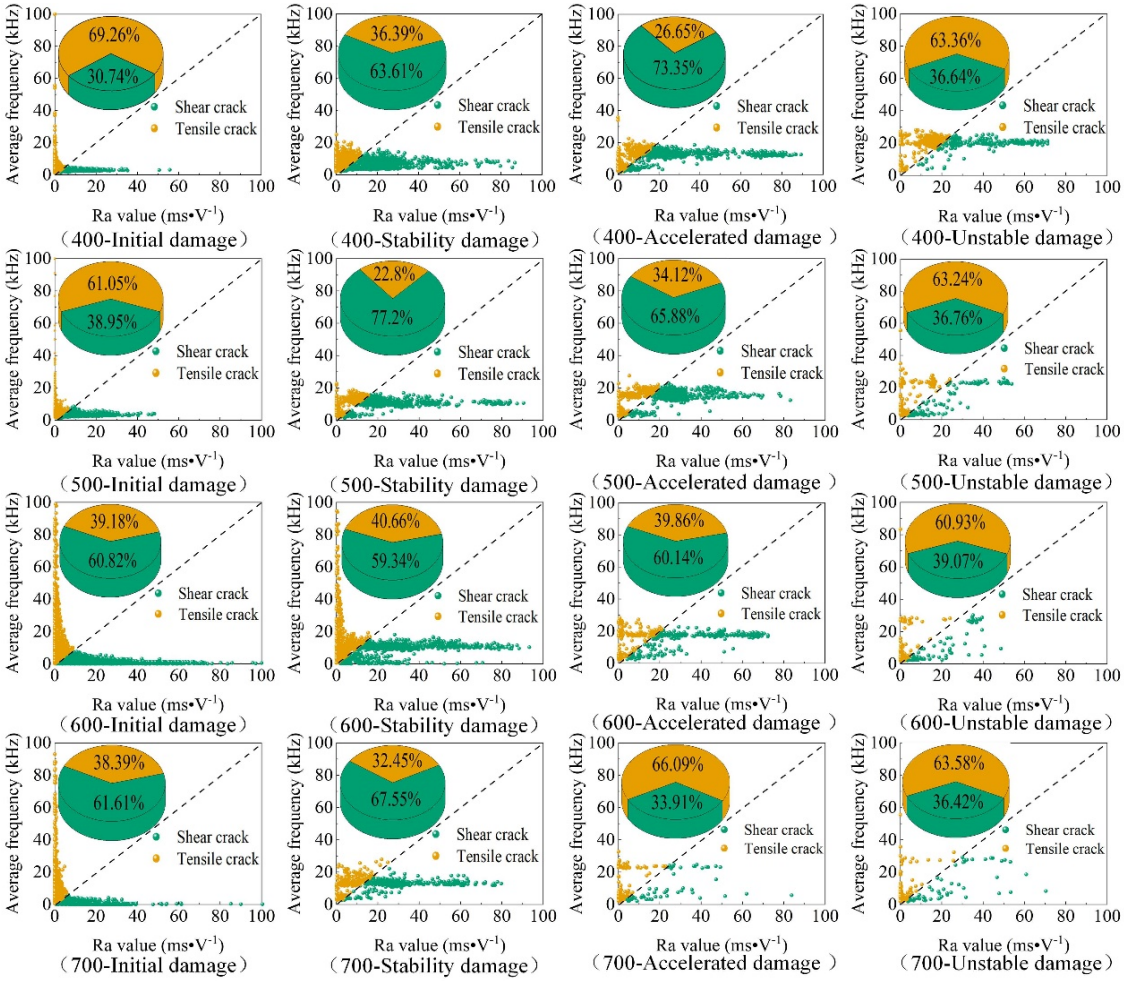

Fig. 7. RA-AF evolution characteristics of foam concrete specimens with different densities

At the initial damage stage, the tensile and shear cracks are still distributed along the two coordinate axes of RA-AF. The average frequency of shear cracks increases slightly, and the full-cycle RA distribution is mainly concentrated below 60 ms•V^{-1} after entering the stable damage stage. The specimens present low RA tensile failure characteristics at the acceleration and unstable damage stages compared with the initial and stable ones. According to the statistics on several full-cycle scatter point events of the specimens with different densities (600 and 700 kg/m^3), the failure form of the high-density specimens shifts from tensile failure to shear failure at the initial damage stage primarily because the cell strength and fiber quantity in the high-density specimens are much higher than those in the low-density specimens. The bearing capacity of the high-density specimens at the initial damage stage mainly originates from the shear resistance of fiber cohesion due to minor porosity and strong fiber cohesion. Additionally, the tensile cracks of the specimen with a density of 700 kg/m^3 at the acceleration and unstable damage stages play a dominant role due to the action of fiber cohesion at the initial and stable damage stages. Fig. 8 shows the crack damage modes of the foam concrete specimens with different densities under vibration load. The specimens with different densities of 400 and 500 kg/m^3 develop tensile cracks first and then shear cracks. The specimen with a density of 600 kg/m^3 first develops shear failure due to fiber cohesion; then, it develops tensile failure after continuous vibration loading with the increase in foam concrete density. The proportion of shear failures at the late stage of the specimen with a density of 700 kg/m^3 decreases, whereas the proportion of tensile failure increases. To sum up, the crack model exerts a noticeable hysteresis effect wherein shear failure mode plays a dominant role gradually at the initial and stable damage stages with the increase in foam concrete density, and the tensile failure mode shifts to the acceleration and unstable damage stages.

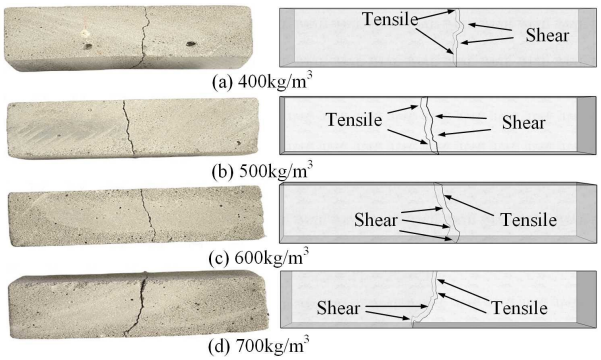

Fig. 8. Crack damage mode of foam concrete with different densities

4.4 Cracking precursor analysis of foam concrete with different densities

The above-mentioned experimental studies demonstrate that peak frequency, duration, amplitude, and AE count have remarkable staged separation effects. The damage laws of foam concrete are analyzed deeply by using peak frequency, amplitude, and duration as the critical parameters to avoid the curse of dimensionality. The corresponding relations between the peak frequency and amplitude of specimens with different densities can be established through K-means clustering analysis, which can provide a novel precursor recognition method for the damage discrimination of foam concrete subgrades under vehicle loads.

K-means clustering analysis evaluates different types of data through the error sum of squares criterion function. Centered at several core zones, data are classified using the error sum of squares until the data points closest to the center region are screened, thus obtaining the optimal clustering results. The function is expressed as

$$J = \sum_{i=1}^{k} \sum_{x=C_i} \left\| m - m_i \right\|^2 \tag{2}$$

where x refers to the data samples, k is the number of clusters, C_i is the sample space of the cluster, and i is the mean vector of the sample space of cluster i.

K-means clustering analysis of AE signals is performed in this study, and the number of clusters is evaluated by the See value. A greatly descending slope indicates a good number of clusters. The cluster number evaluation is shown in Fig. 9.

Fig. 9 shows that the optimal cluster number of foam concrete specimens with different densities (400-700 kg/m^3) is 3. Table 2 shows the AE signal number and clustering results of the foam concrete specimens with different densities. Fig. 10 shows the clustering distributions of the duration, amplitude, and peak frequency of AE signals.

The AE clustering effect of foam concrete with different densities is good. AE amplitude, frequency, and duration generally present a rising trend as the foam concrete density increases. Fig. 10 indicates that the three clusters have explicit boundaries. Cluster 3 has low peak frequency, amplitude, and duration. The peak frequency interval is 1-535 Hz, and apparent boundaries are present among the mid-frequency peak intervals. Moreover, Cluster 3 has the largest number of events among all the clusters in the foam concrete specimens with different densities. Cluster 3 corresponds to the typical matrix cracking damage mode, which initiates from the weak points of specimens and propagates from the substrate cracks to the internal structure of specimens. Cluster 1 has the highest peak frequency, amplitude, and most extended duration among the three clusters. The peak frequency of the specimen with a density of 600 kg/m^3 reaches the maximum (7662 Hz). The specimen with a density of 700 kg/m^3 has the longest duration of 567001 μs and the fewest clustering data points among the specimens. These results are caused by the fact that the peak frequency, amplitude, and duration of Cluster 2 are between those of Clusters 1 and 3. Therefore, Cluster 2 corresponds to cell collapse damage.

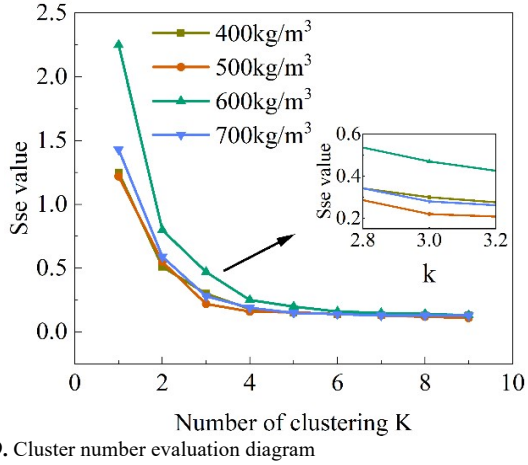

Fig. 9. Cluster number evaluation diagram

Notably, the peak frequency and duration of the specimen with a density of 600 kg/m^3 in Clusters 1 and 2 are greater than those of the specimen with a density of 700 kg/m^3 because the increase in specimen intensity enhances the fiber carrying capacity. By contrast, the fiber breakage and cell collapse degrees are low, thus weakening the high frequency and long duration characteristics. According to the analysis above, the damage modes of foam concrete subgrade with different densities can be recognized comprehensively and effectively through AE amplitude, dominant frequency, and duration under different damage modes. K-means clustering analysis of AE can be used to predict and recognize the damage precursors of foam concrete effectively.

Table 2. Cluster analysis results of specimens

Density/kg/m^3	Parameter	Cluster 1	Cluster 2	Cluster 3
400	Amplitude/dB	26-67	26-59	26-54
	Frequency/Hz	2-5825	1-1047	2-260
	Duration/μs	29639-473108	22214-79669	1-22176
	Quantity	646	2955	7559
500	Amplitude/dB	34-67	26-66	26-41
	Frequency/Hz	5-6684	2-841	1-166
	Duration/μs	82057-473346	22167-81790	1-22150
	Quantity	567	2310	10169
600	Amplitude/dB	35-70	26-70	26-51
	Frequency/Hz	7-7662	1-2747	1-535
	Duration/μs	157464-556726	32036-156599	1-31947
	Quantity	258	2082	5671
700	Amplitude/dB	37-69	26-65	26-52
	Frequency/Hz	1-6646	1-1413	1-198
	Duration/μs	119121-567001	23985-117975	1-23630
	Quantity	289	2228	3387

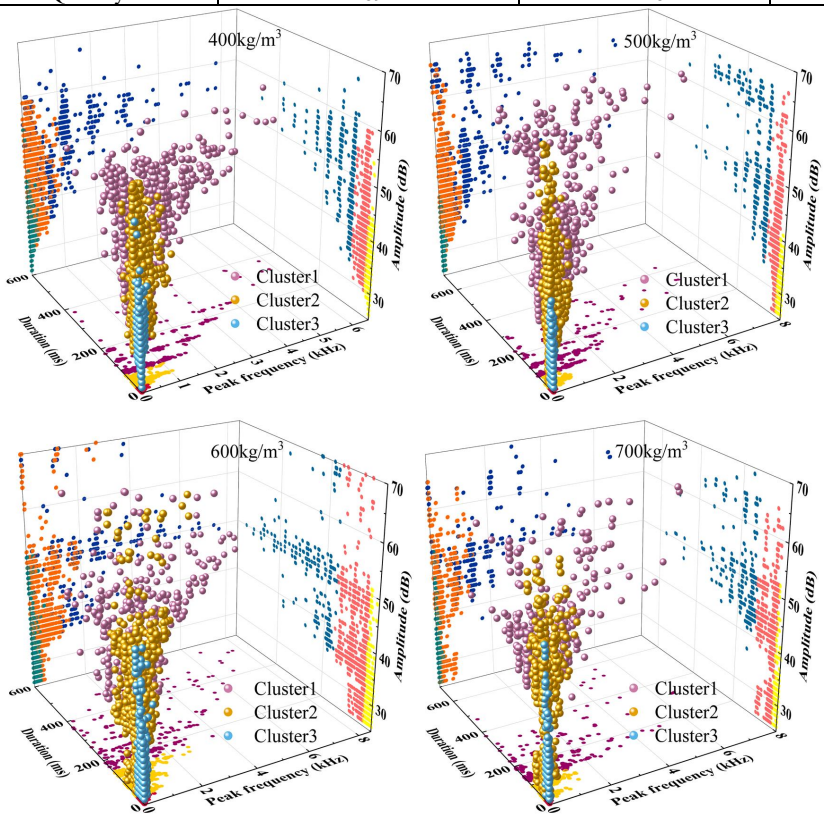

Fig. 10. Acoustic emission clustering diagram of foam concrete with different densities

5. Conclusions

The staged damage characteristics, scale fracture characteristics, and crack propagation mode of foam concrete specimens are analyzed by combining AE parameter information and the microscopic failure mechanisms to examine the vibration failure mechanism and precursor of foam concrete subgrade with different densities. A novel method is proposed to recognize fracture precursors of foam concrete. The following main conclusions can be drawn:

(1) Foam concrete subgrade damage under vibration loads was divided into initial, stable, acceleration, and unstable damage stages. As the density of the foam concrete specimens increases, the foam concrete subgrade shows prominent progressive failure characteristics under vehicle vibration loads. The peak point of the b value of the specimen with a density of 400 kg/m^3 is 2.1, and it increases to 2.9 in the specimen with a density of 700 kg/m^3. The small-scale progressive failure characteristics are gradually strengthened before the critical failure of vehicle loads.

(2) The initial and unstable damage stages of the specimens with different densities (400-500 kg/m^3) are

dominated by tensile cracks. With the increase in density, shear cracks gradually play the dominant role at the initial damage stage of the specimen with a density of 600 kg/m^3, and the shear failure modes move forward gradually. Moreover, tensile failures exert a hysteresis effect because fiber bundle cohesion influences early bearing capacity. Tensile cracks dominate the acceleration damage stage in the specimen with a 700 kg/m^3 density, and tensile failures have a noticeable hysteresis effect.

(3) The AE clustering effect of foam concrete with different densities is good. The peak frequency of Cluster 3 is the lowest and corresponds to substrate cracking. Cluster 1 has the highest peak frequency, amplitude, and most extended duration, which corresponds to the fiber pull-out breakage damage characteristics. The Cluster 2 signals have moderate frequency and amplitude, corresponding to cell collapse damage characteristics. Therefore, the vibration failure modes of foam concrete subgrades with different densities can be identified through AE clustering analysis, which can serve as a novel precursor recognition method for the critical failure of foam concrete subgrades.

Given that the foam concrete subgrade is set as vibration boundaries with fixed supports on both sides in this experiment, the boundaries may need to be further optimized when considering the application positions of vehicle loads in field engineering. Hence, studies on the effects of boundary conditions that are close to field conditions on foam concrete subgrade damage need to be further refined. This refinement can provide a thorough understanding of the mechanical properties of foam concrete backfilled soft subgrades.

Acknowledgements

The authors are grateful for the support provided by the Outstanding Youth Research Program for Universities in Anhui Province (2023AH020025) and the Natural Science Foundation of China (52174105, 52274070).

References

[1] R. Othman, R. P. Jaya, Y. Duraisamy, M. A. Sulaiman, B. W. Chong, and A. Ghamari, "Efficiency of waste as cement replacement in foamed concrete-A Review," *Sustainability*, vol. 15, no. 6, May. 2023, Art. no. 5163.

[2] M. Amran *et al*., "Design efficiency, characteristics, and utilization of reinforced foamed concrete: A Review," *Crystals*, vol. 10, no. 10, Nov. 2020, Art. no. 948.

[3] R. Othman *et al*., "Relation between density and compressive strength of foamed concrete," *Materials*, vol. 14, no. 11, Jul. 2021, Art. no. 2967.

[4] M. Kadela, A. Kukielka, and M. Malek, "Characteristics of lightweight concrete based on a synthetic polymer foaming agent," *Materials*, vol. 13, no. 21, Dec. 2020, Art. no. 4979.

[5] Y. Xu *et al*., "Effect of foam stabilization on the properties of foamed concrete modified by expanded polystyrene," *J. Build. Eng*., vol. 73, Sep. 2023, Art. no. 106822.

[6] P. K. Kumar and K. Chinnaraju, "Comparative experimental investigation on foam concrete with polypropylene fiber and carbon fiber," *Rev. Rom. Mat.*, vol. 52, no. 3, pp. 265-277, Dec. 2022.

[7] F. Batool, M. M. Rafi, and V. Bindiganavile, "Microstructure and thermal conductivity of cement-based foam: A review," *J. Build. Eng.*, vol. 20, pp. 696-704, Oct. 2018.

[8] B. A. Gilka, P. Folino, A. Maier, E. A. B Koenders, and A. Caggiano, "Triaxial failure behavior of highly porous cementitious foams used as heat insulation," *Processes*, vol. 9, no. 8, Sep. 2021, Art. no. 1373.

[9] M. Ben Youssef, K. Miled, and J. Néji, "Mechanical properties of non-autoclaved foam concrete: analytical models vs. experimental data," *Eur. J. Environ. Civ. Eng.*, vol. 24, no. 4, pp. 472-480, Mar. 2020.

[10] M. Frenzel and M. Curbach, "Shear strength of concrete interfaces with infra-lightweight and foam concrete," *Struct. Concr.*, vol. 19, no. 1, pp. 269-283, Dec. 2018.

[11] G. Lacidogna, G. Piana, and A. Carpinteri, "Damage monitoring of three-point bending concrete specimens by acoustic emission and resonant frequency analysis," *Eng. Fract. Mech.*, vol. 210, pp. 203-211, Apr. 2019.

[12] A. A. Ameer, N. H. Thom, and A. R. Dawson, "Pore structure and permeation characteristics of foamed concrete," *J. Adv. Concr. Technol.*, vol. 12, no. 12, pp. 535-544, Apr. 2015.

[13] B. S. Seker, M. Gokce, and K. Toklu, "Investigation of the effect of silica fume and synthetic foam additive on cell structure in ultra-low density foam concrete," *Case Stud. Constr. Mater.*, vol. 16, Jun. 2022, Art. no. e01062.

[14] F. Mendonça, G. Urgessa, and J. Rocco, "Experimental investigation of 50 MPa reinforced concrete slabs subjected to blast loading," *Ing. Invest.*, vol. 38, no. 2, pp. 27-33, Jan. 2019.

[15] X. J. Tan *et al.*, "A combined supporting system based on foamed concrete and U-shaped steel for underground coal mine roadways undergoing large deformations," *Tunn. Undergr. Space Technol.*, vol. 68, pp. 196-210, Sep. 2017.

[16] W. She, Y. S. Zhang, M. R. Jones, and P. P. Guo, "In-situ monitoring the setting behavior of foamed concrete using ultrasonic pulse velocity method," *J. Wuhan Univ. Technol.-Mat. Sci. Edit.*, vol. 28, no. 6, pp. 1146-1154, Jan. 2014.

[17] H. Choi and J. S. Popovics, "NDE application of ultrasonic tomography to a full-scale concrete structure," *IEEE Trans. Ultrason. Ferroelectr. Freq. Control*, vol. 62, no. 6, pp. 1076-1085, Jul. 2015.

[18] J. Feiteira, E. Tsangouri, E. Gruyaert, C. Lors, G. Louis, and N. De belie, "Monitoring crack movement in polymer-based self-healing concrete through digital image correlation, acoustic emission analysis and SEM in-situ loading," *Mater. Des.*, vol. 115, pp. 238-246, Feb. 2017.

[19] Y. F. Hao, G. Z. Yang, and K. K. Li, "Development of fly ash and slag based high-strength alkali-activated foam concrete," *Cem. Concr. Compos.*, vol. 128, Jun. 2022, Art. no. 104447.

[20] D. Falliano, L. Restuccia, and E. Gugliandolo, "A simple optimized foam generator and a study on peculiar aspects concerning foams and foamed concrete," *Constr. Build. Mater.*, vol. 268, Jan. 2021, Art. no. 121101.

[21] Y. Song and D. A. Lange, "Crushing behavior and crushing strengths of low-density foam concrete," *ACI Mater. J.*, vol. 117, no. 2, pp. 43-52, Oct. 2020.

[22] W. H. Zhao, Z. X. Liu, and R. Q. Wang, "Effect of fibers on the mechanical properties and mechanism of cast-in-situ foamed concrete," *Adv. Mater. Sci. Eng.*, vol. 2022, Jun. 2022, Art. no. 2238187.

[23] H. S. Gökçe, N. Öksüzer, H. A. Kamiloğlu, M. Eyuboglu, and F.Yilmaz, "The toughness of polypropylene fiber-reinforced foam Concrete under various uni and triaxial compression loads," *KSCE J. Civ. Eng.*, vol. 27, no. 7, pp. 2982-2992, Jul. 2023.

[24] S. Desutter, S. Verbruggen, T. Tysmans, and D. G. Aggelis, "Fracture monitoring of lightweight composite concrete beams," *Compos. Struct.*, vol. 167, pp. 11-19, Apr. 2017.

[25] M. A. Rasheed, S. S. Prakash, and R. Gangadharan, "Acoustic emission characterization of hybrid fiber reinforced cellular concrete under direct shear loads," *J. Nondestruct. Eval.*, vol. 38, no. 1, Jan. 2019, Art. no. 17.

[26] Z. Z. Lin, C. C. Guo, F. M. Wang, E. Kravchenko, and X. X. Chu, "A typical brittle failure and compression characteristics of polymer based on acoustic emission," *Constr. Build. Mater.*, vol. 392, Jul. 2023, Art. no. 111658.

[27] S. T. Li, X. D. Chen, J. H. Zhang, and W. Dong, "Uniaxial compression failure characteristics of foam concrete with different density grades," (in Chinese), *J. Build. Mater.*, vol. 24, no. 6, pp. 1146-1153, Dec. 2021.

[28] J. H. Gao, Y. J. Xu, and S. C. Yang, "Research on dynamic response of granular base asphalt pavement," (in Chinese), *J. Chongqing Jiaotong Univ.* (*Natural Sci*)., vol. 38, no. 12, pp. 57-62, Dec. 2019.

[29] V. L. Shkuratnik, P. V. Nikolenko, and A. E. Koshelev, "Spectral characteristics of acoustic emission in loaded coal specimens for failure prediction," *J. Min. Sci.*, vol. 53, no. 5, pp. 818-823, Jun. 2018.

[30] E. Agletdinov, D. Merson, and A. Vinogradov, "A new method of low amplitude signal detection and its application in acoustic emission," *Appl. Sci. -Basel.*, vol. 10, no. 1, Mar. 2020, Art. no. 73.

[31] G. G. AGU and C. F. Richter, "Seismicity of the earth and associated phenomena," *J. Geophys. Res.*, vol. 55, no. 1, pp. 97-98, Jan. 1950.

[32] H. R. Li, Z. H. Wang, S. R. Meng, W. G. Zhao, and F. Chen, "Study on damage evolution and acoustic emission activity characteristics of marble under high-temperature triaxial stress," (in Chinese), *Rock Soil Mech.*, vol. 42, no. 10, pp. 2672-2682, Oct. 2021.

[33] V. Tra, K. Jaeyoung, I. Jeong, and K. Jongmyon, "An acoustic emission technique for crack modes classification in concrete structures," *Sustainability*, vol. 12, no. 17, Sep. 2020, Art. no. 6724.

[34] S. Ashraf, S. Khan, and VK. Oad, "Microcracking monitoring and damage detection of graphene nanoplatelets-cement composites based on acoustic emission technology," *Case Stud. Constr. Mater.*, vol. 18, Feb. 2023, Art. no. e01844.